Journal of Materials Chemistry B

PAPER

View Article Online
View Journal | View Issue

Cite this: J. Mater. Chem. B, 2014, 2, 5272

Self-programmed nanovesicle to nanofiber transformation of a dipeptide appended bolaamphiphile and its dose dependent cytotoxic behaviour†

Indrajit Maity,[a] Hamendra S. Parmar,[b] Dnyaneshwar B. Rasale[a] and Apurba K. Das*[a]

Received 5th March 2014
Accepted 16th June 2014

DOI: 10.1039/c4tb00365a

www.rsc.org/MaterialsB

Nanostructural transition of a small peptide bolaamphiphile *via* molecular self-assembly is a challenging task. Here, we report the self-programmed morphological transformation from nanovesicles to nanofibers of a smart peptide bolaamphiphile in its self-assembling hydrogel state. The nanostructural transition occurs based on the structural continuity of the β-sheet structures. Spectroscopic studies confirmed the different molecular arrangements of the two different nanostructures. Furthermore, the smart bolaamphiphile shows a dose-dependent cytotoxicity and cell-proliferation behaviour.

1. Introduction

Precise control in the nanostructural transition of small peptide-based bolaamphiphile molecules *via* molecular self-assembly is a challenging task. Peptide-based nanostructures[1–10] are envisaged through a bottom-up self-assembly approach,[11–15] and they possess a wide range of applications in drug delivery,[16–19] tissue engineering[20–25] and supramolecular electronics.[26–28] However, peptide self-assembly processes are highly sensitive towards changes in stimuli such as pH,[29–31] temperature,[32,33] light,[34] metal ions[35,36] and enzymes.[37–40] The delicate hydrophobic/hydrophilic balance and non-covalent interactions of a molecule are the driving forces for the self-assembly process in a particular solvent, which results in the formation of peptide nanostructures. Stimuli-responsive peptide self-assembly proceeds through an alteration of molecular conformations, which leads to the adoption of different secondary structures. The self-assembly process is dynamic in nature. The dynamic behaviour acts in between the more and relatively less ordered conformational arrangements at the molecular level. Nanostructural transition occurs because of the need to achieve a more stable and ordered molecular arrangement from the loosely ordered arrangement in a particular system. In most of the cases, a change in stimuli directs the morphological transformation from one nanostructure to another. Stimuli-responsive peptide nanofibers have attracted attention because of their potential applications in drug delivery and waste water treatment.[41] The nanostructural transition of peptide into tapes, ribbons, nanofibrils and nanofibers depends on the change in pH.[42] Parquette *et al.* reported peptide-based dendron self-assembly in a controlled manner and the interconversion of nanotubes and fibrillar nanostructures.[43] Direct morphological transformation from twisted ribbons to helical ribbons was reported by Stupp *et al.*[44] The Ulijn group reported a morphological transformation from a micellar solution to a fibrous hydrogel *via* the enzymatic dephosphorylation of a peptide amphiphile.[45] The same group again demonstrated direct enzymatic amide condensation and light induced controlled gelation, which is associated with the morphological transition from a micellar structure to entangled nanofibers.[46] Yang *et al.* tuned the hydrogelation process by the enzymatic dephosphorylation of a small molecule and reported the occurrence of a morphological transformation.[47]

Peptide bolaamphiphiles are an interesting class of organic molecules. In a bolaamphiphile molecule, two terminal hydrophilic groups are attached with a hydrophobic backbone. Shimizu *et al.* demonstrated various types of nanostructure-forming peptide bolaamphiphiles.[48] Nano-doughnut-forming self-assembled peptide bolaamphiphile was also used as a nanoreactor to synthesis Au nanocrystals.[49] The nanostructural transformation requires a stimulus, which can break weak non-covalent interactions and induce another supramolecular arrangement. The change in pH can tune the evolution of different nanostructures of bolaamphiphiles.[50] Here, we report the self-programmed morphological transition from nanovesicles to nanofibers *via* a third polymorphic state of nanocapsules.

[a]Department of Chemistry, Indian Institute of Technology Indore, Indore, India
[b]Department of Biotechnology, Devi Ahilya Vishwavidyalaya, Indore, India. E-mail: apurba.das@iiti.ac.in

† Electronic supplementary information (ESI) available: (1) TEM images of nanovesicles, nanocapsules and nanofibers; (2) AFM images of nanocapsules; (3) Fluorescence and optical microscope images; (4) Synthesis of peptide bolaamphiphile; (5) NMR spectra at different states (nanovesicles and nanofibers) and (6) Statistical analysis of MTT assay. See DOI: 10.1039/c4tb00365a

The cytotoxic study of small molecules has emerged as a promising tool for the development of drugs.[51] Understanding the dose dependent behavior of a small molecule is a crucial and important aspect in the field of biomedicine.[52,53] Hydrogels of small peptide-based molecules are interesting because of their applications in cell-biology.[54] The objectives of this paper are: (a) to incorporate a flexible alkane chain which can give different structures due to conformational heterogeneity, (b) to study the nanostructural transition driven by molecular self-assembly, (c) to understand the mechanism of nanostructural transition with respect to time and (d) to investigate the cytotoxicity and cell proliferation using the self-assembled hydrogel scaffold.

2. Experimental

2.1 Preparation of hydrogel

15 mg (10 mmol L^{-1}) of peptide bolaamphiphile (HO-W-F-Suc-L-W-OH) was dispersed in 2 mL of sodium phosphate buffer solution (pH 8, 10 mmol L^{-1}) and sonicated for 10 minutes. The self-supporting hydrogel was formed after 3 hours.

2.2 General characterization

All NMR characterizations were carried out on a Bruker AV 400 MHz spectrometer at 300 K. Compound concentrations were in the range of 5–10 mmol L^{-1} in $(CD_3)_2SO$ and $CDCl_3$. Mass spectra were recorded on a Bruker micrOTOF-Q II by positive mode electrospray ionisation. Specific rotations of the synthesized compounds were measured on an Autopol V automatic polarimeter (Rudolph Research Analytical). The cell with a length of 100 mm and a capacity of 2 mL was used for this study at 20 °C. For the AFM study, the gel samples were diluted in Milli Q water to a final concentration of 0.5 mmol L^{-1}, placed on a mica slip, and then dried by slow evaporation. Images were obtained with an AIST-NT instrument (model no. smartSPM 1000) using the soft tapping-mode. FT-IR spectra for both the nanovesicles and nanofibers were recorded using a Bruker (Tensor 27) FT-IR spectrophotometer. The gel sample was prepared in D_2O and placed between the crystal Zn–Se windows and scanned between 900 to 4000 cm^{-1} over 64 scans at a resolution of 4 cm^{-1} and at an interval of 1 cm^{-1}. The secondary structure of peptide bolaamphiphile was analyzed with a Jasco J-815 circular dichroism spectrometer. The peptide hydrogel (10 mmol L^{-1}) was diluted to a final concentration of 500 μM in ddH_2O for both the vesicles and nanofibers and measured from 280 nm to 190 nm with a 0.1 data pitch, 20 nm min^{-1} scanning speed, 1 nm band width and 4 s D.I.T. The fluorescence emission spectra of hydrogel (10 mmol L^{-1}) for both the states of nanovesicles and nanofibers were recorded on a Horiba Scientific Fluoromax-4 spectrophotometer with a 1 cm path length quartz cell at room temperature. The slit width for the excitation and emission was set at 2 nm and a 1 nm data pitch. Excitation of the gel sample was performed at 280 nm and the data range was 290 to 500 nm. Data were collected for both the nanostructures of nanovesicles and nanofibers on a Rigaku Smart Lab X-ray diffractometer at a wavelength of 1.5406 Å. X-rays were produced using a sealed tube and were detected using a linear counting detector based on silicon strip technology (Scintillator NaI photomultiplier detector). Fluorescence microscopy experiments were performed on a home-built epifluorescence microscopy set-up. An air-cooled argon ion laser (Melles Griot, model 400-A03) with an excitation wavelength of 500 nm was used to excite the vesicle sample placed on an inverted microscope (Nikon, model Eclipse Ti–U). The laser beam was expanded and subsequently focused on the back-focal plane of an oil immersion objective (100 × 1.49 NA Nikon) to illuminate a 60 × 60 μm^2 area of the sample. The PL from the sample was recorded by a B2A filter cube (Nikon) with a 505 nm dichroic mirror and a 520 nm long-pass filter and finally imaged with a back-illuminated EMCCD camera (Andor, model iXon X3 897) at an exposure time of 300 ms. The images were analyzed with an ImageJ (Version 1.46r) NIH. Optical microscopy images were taken with a Zeiss AxioCam ERc5s microscope using 40 × magnification. The peptide bolaamphiphile vesicles and Congo red loaded vesicles were diluted in double distilled water and the samples were prepared by depositing a few drops on a cover slip.

2.3 Cell culture (MTT assay)

Total WBCs were isolated from chicken blood. The 1×10^6 mL^{-1} concentration of cells was taken from 100 μL in each well. A 20 mmol L^{-1} concentration of hydrogel stock solution was used to prepare the final concentrations of 10–100% in different wells (each in triplicate) at a pH of 7.4. Commercially available kit from Hi-Media Pvt. Ltd., Mumbai was used to conduct the MTT assay. Cells were mixed with the hydrogel and incubated for 48 hours with the hydrogel or in media (control). The minimum essential media without phenol red was used to culture the cells. After culturing the cells, the MTT reagent was added to each well. After 4 hours, the MTT solution was carefully removed and the purple crystals were solubilized in DMSO. The optical density of the reagent was then measured at a wavelength of 570 nm with a reference wavelength of 650 nm. The effect on cell viability or number was calculated in percentages, considering the average absorbance value from the control samples to be 100%.

2.4 Statistical analysis

Data are expressed as mean ± SEM and were analyzed by the analysis of variance (ANOVA) followed by a post hoc Newman–Keuls multiple comparison test using a trial version of Prism 5 software for Windows (GraphPad Software, Inc., La Jolla, CA, USA).

3. Results and discussion

We synthesized a peptide bolaamphiphile HO-W-F-Suc-L-W-OH (W: tryptophan, L: leucine, F: phenylalanine and Suc: succinic acid) with a centrally located flexible succinic acid moiety. 15 mg of peptide bolaamphiphile (10 mmol L^{-1}) was dispersed in 2 mL of phosphate buffer (pH = 8, 10 mM). A self-supporting hydrogel was achieved by successive sonication, and was used

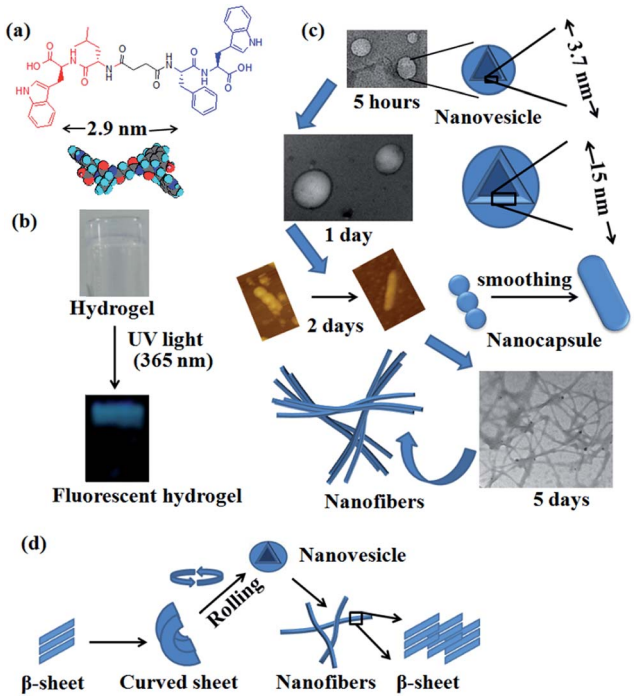

Scheme 1 (a) Molecular structure of peptide bolaamphiphile, (b) the self-supporting peptide bolaamphiphile hydrogel under daylight which emits blue light upon irradiation at 365 nm UV light, (c) self-programmed morphological transformation from nanovesicles to nanofibers through a third polymorphic capsular nanostructure, and (d) the scheme representing the formation of β-sheets, which form vesicles *via* a rolling up of the sheet, and then nanofibers are formed *via* a reorientation of the β-sheets.

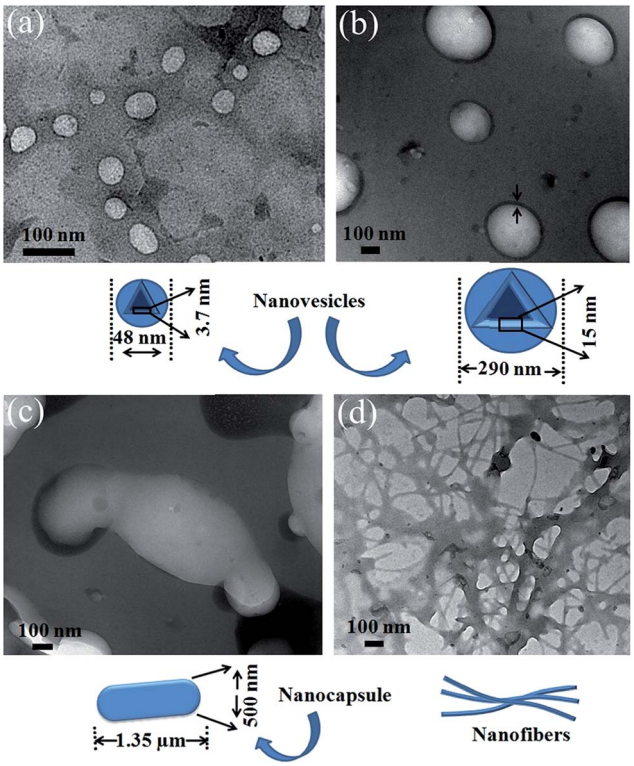

Fig. 1 TEM images showing the nanostructural evolution of (a) nanovesicles at 5 hours, (b) multilayered nanovesicles at 1 day, (c) nanocapsules at 2 days and (d) nanofibrillar structures at 5 days of hydrogelation.

to investigate the morphological transformation (Scheme 1). The critical gelation concentration of the precursor was found to be 8 mmol L^{-1}. The self-programmed nanostructural transition from nanovesicle to nanofiber of hydrogel 1 (10 mmol L^{-1}) with a self-assembly mechanism with respect to time was investigated by transmission electron microscopy (TEM) and atomic force microscopy (AFM).

The transmission electron microscopy image (Fig. 1) showed that the peptide bolaamphiphile self assembled to form nanovesicles within 5 hours of hydrogelation. At this early stage, the evolution of nanovesicles[55] occurred through a loose molecular arrangement of the self-assembled molecules (ESI, Fig. S1†). The TEM image revealed the average diameter of the nanovesicles to be 48 nm. The average wall thickness of these nanovesicles is 3.7 nm (Scheme 1). At day 1, the TEM image showed that the early evolved nanovesicles became larger in size and the average diameter was found to be 290 nm. The average wall thickness was estimated from the TEM image, and was observed to be 15 nm. The vesicle-wall was formed by a multilamellar arrangement of self-assembled molecules, which adopted a loose β-sheet-like structure. At day 2, a nanocapsule-like nanostructure was observed with an increased dimension. The length of the capsule was about 1.35 μm and the diameter was around 500 nm at the middle of the nanostructure. At this stage, the association of two or more nanovesicles was also observed. It is evident that the nanocapsule-like nanostructure evolved from the association of the nanovesicles (Fig. 2). Nanofibrillar structures[31] were observed after 4 days of hydrogelation. The TEM image showed that the nanofibrillar network structures were formed from previously collapsed nanostructures, and the nucleation point was clearly observed in the TEM image. The nanofibers were several micrometers in length and the average diameter of the nanofiber was 12 nm. At this stage, no nanovesicle was found, which indicates the complete conversion of nanovesicles to nanofibers (ESI, Fig. 2†).

The atomic force microscopy (AFM) images[56,57] (Fig. 3) were also showed a similar trend as the TEM images. The peptide bolaamphiphile molecules self assembled into nanovesicles at an early stage. The size of the nanovesicles after 5 hours of hydrogelation was in the range of 45 to 150 nm. After that, the nanovesicles fused with each other to form cocoon-like nanostructures. The average diameter of these nanostructures was 300 nm. At 2 days of self-assembly, the cocoon-like nanostructures transformed into nanocapsule-like structures, which were 0.6 to 1.3 μm in length. The average diameter of these nanocapsules was 500 nm and the height was in the range of 5 to 10 nm (ESI, Fig. S3†). At 5 days of sonication, nanofibers were formed. The diameter of the nanofiber was 20 nm. The self-assembly process was initiated by sonication but the morphological transition from nanovesicles to nanofibers occurred by a self-programmed process of smart bolaamphiphile.

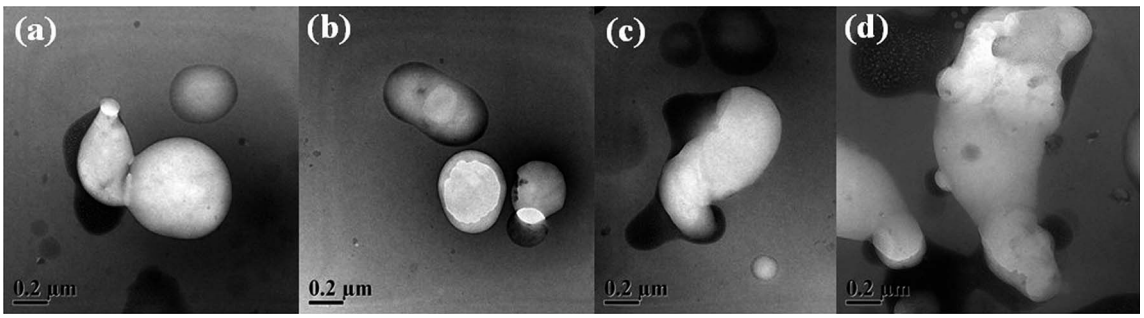

Fig. 2 TEM images showing the formation of nanocapsules from the association of nanovesicles. TEM images showing the (a) association of two vesicles towards the formation of a nanocapsule, (b)–(d) show the self-assembled peptide bolaamphiphile nanocapsules at 2 days.

The hollow nature of the nanovesicles was proven by the Congo red dye encapsulation experiment.[58] An aqueous solution (2 mg mL^{-1}) of the Congo red dye was prepared and added to the vesicles. These vesicles entrapped the Congo red dye within a period of 4 and 5 hours. After 5 hours, the fluorescence microscopy images (Fig. 4) clearly demonstrated that the physiological dye, Congo red, was successfully encapsulated inside the vesicles. In addition to the fluorescence microscopy images, the optical microscopy images[59] also showed the vesicle structure of the peptide bolaamphiphile hydrogel at 1 day of self-assembly (ESI, Fig. 4†).

From the abovementioned observations, we were interested in elucidating the differences in molecular arrangement at the supramolecular level inside these two different nanostructures. To gain more insight into the molecular conformations of the two different nanostructures, several spectroscopic analyses were performed. FTIR studies were carried out at day 1 and 5 of the hydrogelation to understand the secondary structures adopted by the self-assembled peptide bolaamphiphiles inside the two different nanostructures. At day 1, two peaks appeared at 1646 cm^{-1} and 1714 cm^{-1} for the hydrogel enriched with nanovesicles. The peak at 1714 cm^{-1} suggested that the carboxylic acid groups are involved in hydrogen bonding interactions, whereas the appearance of a characteristic amide I peak at 1646 cm^{-1} revealed a type of β-sheet arrangement.[60] At day 5, several characteristic peaks appeared for the hydrogel consisting of nanofibrillar morphology. The C═O stretching band at 1702 cm^{-1} indicated a hydrogen bonded carboxylic acid functionality in the peptide nanofibers. The amide I band at 1635 cm^{-1}, along with a weak shoulder at 1608 cm^{-1}, revealed that the peptide bolaamphiphile molecules are self-assembled into a hydrogen bonded β-sheet arrangement[9] in the nanofibers (Fig. 5a). From the FTIR spectra, it is clear that the molecular packing is more ordered and more compact in the β-sheet arrangement for the nanofibers rather than for the nanovesicles.

The difference in the molecular conformations inside the two different nanostructures at two different stages of self-assembly was examined by circular dichroism (CD) spectroscopy (Fig. 5b).[61,62] For both the cases, the hydrogels were diluted to 500 μM concentration in ddH_2O to investigate the secondary structures of the two different nanostructures. The CD spectrum of the nanovesicles showed a characteristic negative peak around 201 nm with a weak shoulder at 211 nm, which resulted from the n–π* transition of the CO–NH groups of the peptide bolaamphiphile molecule. This CD signature represented a coil-type β-sheet arrangement of peptide bolaamphiphiles in the nanovesicle. Another strong positive band appeared at 226 nm, which is responsible for the electron-transfer of the non-bonding electron of the nitrogen atom into the π* orbital system of the indole ring of the tryptophan moiety.[63] The CD spectrum for the nanofibers showed a characteristic negative band at 216 nm with a weak negative band at 201 nm for the n–π* transition of the CO–NH groups. This CD signature confirmed the hydrogen bonded β-sheet arrangement, which is

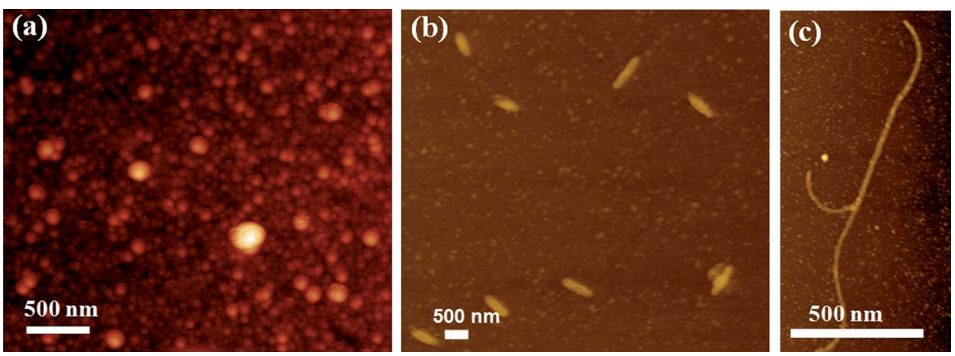

Fig. 3 AFM images showing the nanostructural evolution of (a) nanovesicles at 1 day, (b) nanocapsules at 2 days and (c) nanofibrillar structures at 5 days of hydrogelation.

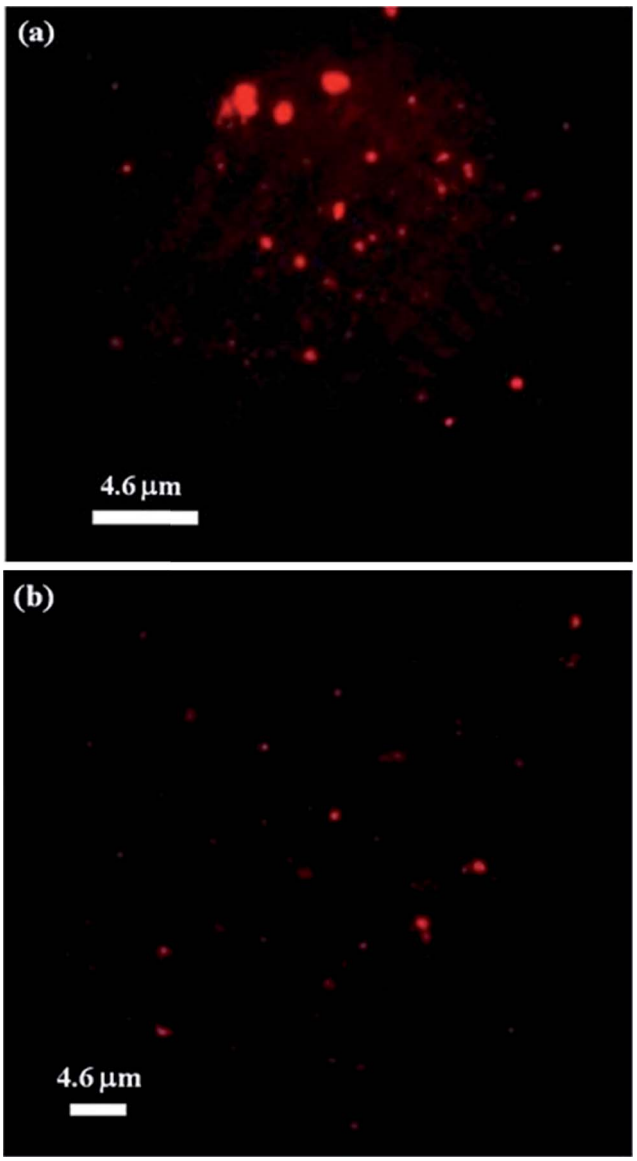

Fig. 4 Fluorescence microscopic images showing the encapsulation of a physiological dye, Congo red, by nanovesicles.

more ordered for nanofibers than nanovesicles. Another positive band at 229 nm appeared because of the tryptophan moiety, which was slightly red shifted with an increase in ellipticity from the corresponding peak for the nanovesicles. This occurred from the extended π–π stacking interactions of the tryptophan aromatic rings during the self-assembly process to form nanofibers.

The fluorescence spectroscopy technique was also exploited to explore π–π stacking interactions during the self-assembly process of peptide bolaamphiphile and to understand the role of the aromatic moieties of peptide bolaamphiphile during structural transition from nanovesicles to nanofibers (Fig. 5c). The fluorescence spectra showed that the nanovesicles emitted at 353 nm, whereas the nanofibers showed an emission maxima at 357 nm upon excitation at 280 nm. The emission peak for both the cases resulted from the tryptophan moiety of the self-assembled bolaamphiphile molecules. The 4 nm red shift of the emission maxima occurred from the nanostructural transition of nanovesicles to nanofibers, which suggests that the peptide bolaamphiphiles are arranged into more ordered and compact β-sheet structures through the synergic effects of hydrogen bonding and extended π–π stacking interactions of the tryptophan residues inside the nanofibers.[9]

The powder X-ray diffraction (PXRD) data (Fig. 5d) clearly revealed the conformational differences between the two morphological states of nanovesicles and nanofibers. For the nanovesicles, the characteristic peak at $2\theta = 18.96^\circ$, corresponding to a d spacing of 4.67 Å, was observed. The peak at 4.67 Å is related to the spacing between the two peptide bolaamphiphiles in a β-sheet arrangement.[64] For the nanofibers, a signal at $2\theta = 20.15^\circ$, corresponding to a d spacing of 4.40 Å, was observed, which is related to the spacing between the two successive peptide backbones in a β-sheet arrangement. In addition, several reflections were observed in the 2θ range of 4–11°, which result from the ordered stacking periodicity of a β-sheet.[55] A typical peak at $2\theta = 10.31^\circ$, corresponding to a d spacing of 8.56 Å, revealed the distance between the two successive β-sheets. The powder X-ray diffraction data clearly demonstrated that the peptide bolaamphiphiles are self-assembled into a more ordered β-sheet arrangement inside the nanofibers rather than the nanovesicles.

To obtain more structural information, the hydrogel at two different states was characterized by ^{1}H and 2D NMR spectroscopy. Nanovesicle and nanofiber enriched hydrogels were lyophilized and characterized by NMR in DMSO-d6 (ESI, Fig. S8–S13†). All the ^{1}H NMR, ^{1}H-^{1}H COSY and ROESY spectra showed similar patterns for both the nanovesicle and nanofiber states. The ROESY spectra (ESI, Fig. S11 and S13†) for both the states showed that the tryptophan amide–CONH–protons are interacting with the –CH_2–protons of the succinic moiety. The NMR results demonstrated the twisting conformation of the self-assembled peptide bolaamphiphile in the hydrogel phase for both the nanostructures. Here, we proposed a mechanism for the self-assembly process, which formulates the nanostructural transition from nanovesicles to nanofibers. Fig. 1d gives a schematic representation of the morphological transformation. At an early stage, self-assembly leads to the formation of β-sheets, which form a curved sheet by a higher ordered self-assembly. Two-dimensional curved sheets result in the formation of nanovesicle structures.[65] After 4 days, nanofibrous morphology is formed *via* a reorientation of the stable β-sheet structures.

Cellular toxicity and proliferation studies with peptide-based materials have attracted increased research interest in the field of biomedicine and biotechnology.[66,67] We investigated the cytotoxic and biocompatible behaviour with the cell proliferation of this peptide bolaamphiphile. For this investigation, we cultured WBC (white blood corpuscle) cells with different concentrations of hydrogel. Total WBCs were isolated from chicken blood. A 20 mmol L^{-1} concentration of hydrogel stock solution was used to prepare the final concentrations of 10–100% in different wells (each in triplicate). Cells were incubated for 48 hours with the hydrogel solution and in media for the control experiment. The minimum essential media without

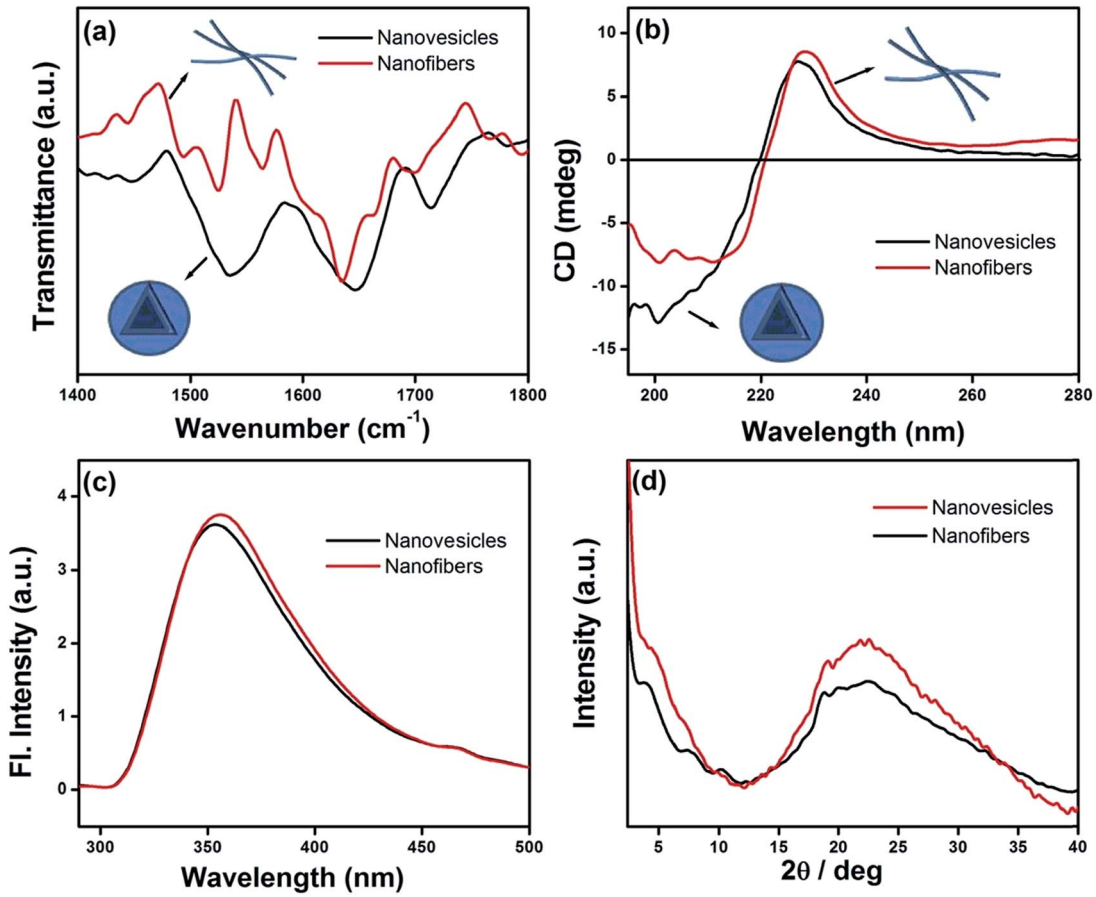

Fig. 5 (a) FTIR, (b) CD and (c) fluorescence spectra (concentration: 10 mmol L^{-1}, $\lambda_{ex} = 280$ nm) for both the nanostructures of nanovesicles and nanofibers. The spectroscopic studies confirm a more compact β-sheet arrangement inside the nanofibers rather than nanovesicles through the synergistic effect of hydrogen bonding and π–π stacking interactions. (d) PXRD for both the nanovesicles and nanofibers confirm the loose molecular arrangement inside the nanovesicles and a more compact molecular arrangement inside the nanofibers.

phenol red was used to culture the cells. The effects on cell viability were calculated in percentages, considering the average absorbance value from the control samples to be 100%. The data from Table 1 shows that the cell viability and cell proliferation occurred at 40% and 50% hydrogel concentrations but the maximum increase in cell viability was found at a 50% concentration of hydrogel solution. The 30% concentration of hydrogel solution appeared to be safe but the rest of the concentrations were found to be either too suboptimal to exert any substantial effects or toxic (at higher doses). Data from the MTT assay (ESI†) consistently revealed the dose dependency of the used hydrogel as the best effect, which was observed at 50% media supplementation by hydrogel. Lower concentrations proved to be less effective and higher concentrations were found to be toxic in nature. The replacement of 50% of the culture media by hydrogel was most effective for cell proliferation. Cell viability suggested that the use of hydrogel along with media may be suitable to prevent toxicity and to increase viability and cell growth. Similar effects on cellular viability and membrane fluidity were also observed earlier for drug compounds and herbal extracts.[68–70]

Table 1 Evaluation of hydrogel preparation on cell viability and proliferation using MTT (3-[4,5-dimethylthiazol-2-yl]-2,5-diphenyl tetrazolium bromide) cell assay[a]

Percentage viability as compare to control	% of hydrogel
77.983 ± 2.608^{aa}	10
91.126 ± 2.310^{bb}	20
99.69 ± 1.862^{bb}	30
126.293 ± 1.184^{cc}	40
197.126 ± 4.063^{dd}	50
95.82 ± 2.263^{be}	60
93.26 ± 1.330^{be}	70
92.656 ± 2.343^{be}	80
49.843 ± 1.222^{ff}	90
35.47 ± 1.102^{gg}	100

[a] Values are the mean ± SE of three measurements. Means in columns without letters in common differ significantly ($P \leq 0.05$).

4. Conclusions

In summary, we describe a sonication-induced phenylalanine and tryptophan-rich peptide bolaamphiphile self-assembly

through the synergistic effects of H-bonding and π–π stacking interactions. The self-assembling peptide bolaamphiphiles form self-supporting nanostructured fluorescent hydrogel. The self-programmed nanostructural transition from nanovesicles to the nanofibers of peptide bolaamphiphiles occurs through the structural continuity of stable β-sheets. The real time nanostructural transition was examined by TEM and AFM. The molecular conformations and arrangements for both the cases were investigated thoroughly by various spectroscopic techniques. The spectroscopic studies suggest loose β-sheet arrangements of peptide bolaamphiphiles inside the vesicles. Moreover, peptide bolaamphiphiles are self-assembled into more ordered and compact β-sheet arrangements inside the nanofibers. Furthermore, the peptide bolaamphiphile shows dose-dependent cytotoxic and cell-proliferation behaviour.

Acknowledgements

AKD would like to acknowledge CSIR, New Delhi, India for financial support. IM and DBR are indebted to CSIR, New Delhi, India for their fellowship for this work.

Notes and references

1 R. Ni, W. S. Childers, K. I. Hardcastle, A. K. Mehta and D. G. Lynn, *Angew. Chem., Int. Ed.*, 2012, **51**, 6635–6638.
2 S. Yuran, Y. Razvag and M. Reches, *Acs Nano*, 2012, **6**, 9559–9566.
3 C. Reiriz, R. J. Brea, R. Arranz, J. L. Carrascosa, A. Garibotti, B. Manning, J. M. Valpuesta, R. Eritja, L. Castedo and J. R. Granja, *J. Am. Chem. Soc.*, 2009, **131**, 11335–11337.
4 A. Montero, J. M. Beierle, C. A. Olsen and M. R. Ghadiri, *J. Am. Chem. Soc.*, 2009, **131**, 3033–3041.
5 S. Scanlon and A. Aggeli, *Nano Today*, 2008, **3**, 22–30.
6 S. Santoso, W. Hwang, H. Hartman and S. Zhang, *Nano Lett.*, 2002, **2**, 687–691.
7 H. R. Marsden, J.-W. Handgraaf, F. Nudelman, N. A. J. M. Sommerdijk and A. Kros, *J. Am. Chem. Soc.*, 2010, **132**, 2370–2377.
8 J. B. Matson, C. J. Newcomb, R. Bitton and S. I. Stupp, *Soft Matter*, 2012, **8**, 3586–3595.
9 I. Maity, D. B. Rasale and A. K. Das, *Soft Matter*, 2012, **8**, 5301–5308.
10 E. Lee, J.-K. Kim and M. Lee, *Angew. Chem., Int. Ed.*, 2008, **47**, 6375–6378.
11 J. J. D. de Jong, L. N. Lucas, R. M. Kellogg, J. H. van Esch and B. L. Feringa, *Science*, 2004, **304**, 278–281.
12 M. D. Segarra-Maset, V. J. Nebot, J. F. Miravet and B. Escuder, *Chem. Soc. Rev.*, 2013, **42**, 7086–7098.
13 R. V. Ulijn and A. M. Smith, *Chem. Soc. Rev.*, 2008, **37**, 664–675.
14 T. Rehm and C. Schmuck, *Chem. Commun.*, 2008, 801–813.
15 K. H. Smith, E. Tejeda-Montes, M. Poch and A. Mata, *Chem. Soc. Rev.*, 2011, **40**, 4563–4577.
16 J. Kopecek and J. Yang, *Angew. Chem., Int. Ed.*, 2012, **51**, 7396–7417.
17 J. V. Georgieva, R. P. Brinkhuis, K. Stojanov, C. A. G. M. Weijers, H. Zuilhof, F. P. J. T. Rutjes, D. Hoekstra, J. C. M. van Hest and I. S. Zuhorn, *Angew. Chem., Int. Ed.*, 2012, **51**, 8339–8342.
18 J. Naskar, G. Palui and A. Banerjee, *J. Phys. Chem. B*, 2009, **113**, 11787–11792.
19 Y.-B. Lim, E. Lee, Y.-R. Yoon, M. S. Lee and M. Lee, *Angew. Chem., Int. Ed.*, 2008, **47**, 4525–4528.
20 N. S. Kehr, E. A. Prasetyanto, K. Benson, B. Ergun, A. Galstyan and H.-J. Galla, *Angew. Chem., Int. Ed.*, 2013, **52**, 1156–1160.
21 C. A. DeForest and K. S. Anseth, *Angew. Chem., Int. Ed.*, 2012, **51**, 1816–1819.
22 M. J. Webber, J. Tongers, C. J. Newcomb, K.-T. Marquardt, J. Bauersachs, D. W. Losordo and S. I. Stupp, *Proc. Natl. Acad. Sci. U. S. A.*, 2011, **108**, 13438–13443.
23 B. Tian, J. Liu, T. Dvir, L. Jin, J. H. Tsui, Q. Qing, Z. Suo, R. Langer, D. S. Kohane and C. M. Lieber, *Nat. Mater.*, 2012, **11**, 986–994.
24 D. Seliktar, *Science*, 2012, **336**, 1124–1128.
25 F. G. Omenetto and D. L. Kaplan, *Science*, 2010, **329**, 528–531.
26 A. R. Hirst, B. Escuder, J. F. Miravet and D. K. Smith, *Angew. Chem., Int. Ed.*, 2008, **47**, 8002–8018.
27 S. Roy, D. K. Maiti, S. Panigrahi, D. Basak and A. Banerjee, *RSC Adv.*, 2012, **2**, 11053–11060.
28 H. Xu, A. K. Das, M. Horie, M. S. Shaik, A. M. Smith, Y. Luo, X. Lu, R. Collins, S. Y. Liem, A. Song, P. L. A. Popelier, M. L. Turner, P. Xiao, I. A. Kinloch and R. V. Ulijn, *Nanoscale*, 2010, **2**, 960–966.
29 C. Whitehouse, J. Fang, A. Aggeli, M. Bell, R. Brydson, C. W. G. Fishwick, J. R. Henderson, C. M. Knobler, R. W. Owens, N. H. Thomson, D. A. Smith and N. Boden, *Angew. Chem., Int. Ed.*, 2005, **44**, 1965–1968.
30 T. H. Larsen, M. C. Branco, K. Rajagopal, J. P. Schneider and E. M. Furst, *Macromolecules*, 2009, **42**, 8443–8450.
31 I. Maity, D. B. Rasale and A. K. Das, *RSC Adv.*, 2013, **3**, 6395–6400.
32 D. J. Pochan, J. P. Schneider, J. Kretsinger, B. Ozbas, K. Rajagopal and L. Haines, *J. Am. Chem. Soc.*, 2003, **125**, 11802–11803.
33 A. Sanchez-Ferrer, V. K. Kotharangannagari, J. Ruokolainen and R. Mezzenga, *Soft Matter*, 2013, **9**, 4304–4311.
34 L. A. Haines, K. Rajagopal, B. Ozbas, D. A. Salick, D. J. Pochan and J. P. Schneider, *J. Am. Chem. Soc.*, 2005, **127**, 17025–17029.
35 D. W. P. M. Lowik, E. H. P. Leunissen, M. van den Heuvel, M. B. Hansen and J. C. M. van Hest, *Chem. Soc. Rev.*, 2010, **39**, 3394–3412.
36 T. Yucel, C. M. Micklitsch, J. P. Schneider and D. J. Pochan, *Macromolecules*, 2008, **41**, 5763–5772.
37 Z. Yang, G. Liang and B. Xu, *Acc. Chem. Res.*, 2008, **41**, 315–326.
38 J. Hu, G. Zhang and S. Liu, *Chem. Soc. Rev.*, 2012, **41**, 5933–5949.
39 D. B. Rasale, I. Maity and A. K. Das, *RSC. Adv.*, 2012, **2**, 9791–9794.

40 A. K. Das, R. Collins and R. V. Ulijn, *Small*, 2008, **4**, 279–287.
41 S. Ray, A. K. Das and A. Banerjee, *Chem. Mater.*, 2007, **19**, 1633–1639.
42 A. Aggeli, M. Bell, L. M. Carrick, C. W. G. Fishwick, R. Harding, P. J. Mawer, S. E. Radford, A. E. Strong and N. Boden, *J. Am. Chem. Soc.*, 2003, **125**, 9619–9628.
43 H. Shao and J. R. Parquette, *Angew. Chem., Int. Ed.*, 2009, **48**, 2525–2528.
44 E. T. Pashuck and S. I. Stupp, *J. Am. Chem. Soc.*, 2010, **132**, 8819–8821.
45 J. W. Sadownik, J. Leckie and R. V. Ulijn, *Chem. Commun.*, 2011, **47**, 728–730.
46 J. K. Sahoo, S. K. M. Nalluri, N. Javid, H. Webb and R. V. Ulijn, *Chem. Commun.*, 2014, **50**, 5462–5464.
47 J. Gao, H. Wang, L. Wang, J. Wang, D. Kong and Z. Yang, *J. Am. Chem. Soc.*, 2009, **131**, 11286–11287.
48 T. Shimizu, M. Masuda and H. Minamikawa, *Chem. Rev.*, 2005, **105**, 1401–1443.
49 R. Djalali, J. Samson and H. Matsui, *J. Am. Chem. Soc.*, 2004, **126**, 7935–7939.
50 T. Wang, J. Jiang, Y. Liu, Z. Li and M. Liu, *Langmuir*, 2010, **26**, 18694–18700.
51 N. Krall, J. Scheuermann and D. Neri, *Angew. Chem., Int. Ed*, 2013, **52**, 1384–1402.
52 F. von Nussbaum, M. Brands, B. Hinzen, S. Weigand and D. Habich, *Angew. Chem., Int. Ed.*, 2006, **45**, 5072–5129.
53 A. Kwiatkowska, F. Couture, C. Levesque, K. Ly, R. Desjardins, S. Beauchemin, A. Prahl, B. Lammek, W. Neugebauer, Y. L. Dory and R. Day, *J. Med. Chem.*, 2014, **57**, 98–109.
54 A. Baral, S. Roy, A. Dehsorkhi, I. W. Hamley, S. Mohapatra, S. Ghosh and A. Banerjee, *Langmuir*, 2014, **30**, 929–936.
55 D. Ke, C. Zhan, A. D. Q. Li and J. Yao, *Angew. Chem., Int. Ed.*, 2011, **50**, 3715–3719.
56 S. Ghosh, M. Reches, E. Gazit and S. Verma, *Angew. Chem., Int. Ed.*, 2007, **46**, 2002–2004.
57 D. B. Rasale, I. Maity, M. Konda and A. K. Das, *Chem. Commun.*, 2013, **49**, 4815–4817.
58 P. P. Bose, A. K. Das, R. P. Hegde, N. Shamala and A. Banerjee, *Chem. Mater.*, 2007, **19**, 6150–6157.
59 K. Sun, K. Chen, G. Xue, J. Cai, G. Zou, Y. Li and Q. Zhang, *RSC Adv.*, 2013, **3**, 23997–24000.
60 J. T. Pelton and L. R. McLean, *Anal. Biochem.*, 2000, **277**, 167–176.
61 S. Datta, S. K. Samanta and S. Bhattacharya, *Chem.–Eur. J.*, 2013, **19**, 11364–11373.
62 X. Yan, Y. Cui, Q. He, K. Wang and J. Li, *Chem. Mater.*, 2008, **20**, 1522–1526.
63 I. Maity, M. K. Manna, D. B. Rasale and A. K. Das, *ChemPlusChem.*, 2014, **79**, 413–420.
64 K. L. Morris, S. Zibaee, L. Chen, M. Goedert, P. Sikorski and L. C. Serpell, *Angew. Chem., Int. Ed.*, 2013, **125**, 2335–2339.
65 J. Naskar and A. Banerjee, *Chem.–Asian J.*, 2009, **4**, 1817–1823.
66 V. Jayawarna, M. Ali, T. A. Jowitt, A. F. Miller, A. Saiani, J. E. Gough and R. V. Ulijn, *Adv. Mater.*, 2006, **18**, 611–614.
67 Y. Kuang and B. Xu, *Angew. Chem., Int. Ed.*, 2013, **52**, 6944–6948.
68 H. S. Parmar and A. Kar, *J. Med. Food.*, 2008, **11**, 376–381.
69 H. S. Parmar and A. Kar, *Drug Discoveries Ther.*, 2009, **3**, 49–55.
70 A. Sethi, H. S. Parmar and A. Kumar, *Basic Clin. Pharmacol. Toxicol.*, 2011, **108**, 371–377.